



# First principles study of structural, vibrational and electronic properties of graphene-like $\text{MX}_2$ ( $\text{M}=\text{Mo}, \text{Nb}, \text{W}, \text{Ta}$ ; $\text{X}=\text{S}, \text{Se}, \text{Te}$ ) monolayers

Yi Ding<sup>a,\*</sup>, Yanli Wang<sup>b,\*</sup>, Jun Ni<sup>c</sup>, Lin Shi<sup>d</sup>, Siqi Shi<sup>b</sup>, Weihua Tang<sup>b</sup>

<sup>a</sup> Department of Physics, Hangzhou Normal University, Hangzhou, Zhejiang 310036, People's Republic of China

<sup>b</sup> Department of Physics, Center for Optoelectronics Materials and Devices, Zhejiang Sci-Tech University, Xiasha College Park, Hangzhou, Zhejiang 310018, People's Republic of China

<sup>c</sup> Department of Physics, Key Laboratory of Atomic and Molecular Nanoscience (Ministry of Education), Tsinghua University, Beijing 100084, People's Republic of China

<sup>d</sup> Suzhou Institute of Nano-Tech and Nano-Bionics, Chinese Academy of Sciences, Suzhou 215125, People's Republic of China

## ARTICLE INFO

### Article history:

Received 25 January 2011

Received in revised form

17 March 2011

Accepted 18 March 2011

Available online 23 March 2011

### Keywords:

Graphene-like structure

Electronic structure

First principles calculation

## ABSTRACT

Using first principles calculations, we investigate the structural, vibrational and electronic structures of the monolayer graphene-like transition-metal dichalcogenide ( $\text{MX}_2$ ) sheets. We find the lattice parameters and stabilities of the  $\text{MX}_2$  sheets are mainly determined by the chalcogen atoms, while the electronic properties depend on the metal atoms. The  $\text{NbS}_2$  and  $\text{TaS}_2$  sheets have comparable energetic stabilities to the synthesized  $\text{MoS}_2$  and  $\text{WS}_2$  ones. The molybdenum and tungsten dichalcogenide ( $\text{MoX}_2$  and  $\text{WX}_2$ ) sheets have similar lattice parameters, vibrational modes, and electronic structures. These analogies also exist between the niobium and tantalum dichalcogenide ( $\text{NbX}_2$  and  $\text{TaX}_2$ ) sheets. However, the  $\text{NbX}_2$  and  $\text{TaX}_2$  sheets are metals, while the  $\text{MoX}_2$  and  $\text{WX}_2$  ones are semiconductors with direct-band gaps. When the Nb and Ta atoms are doped into the  $\text{MoS}_2$  and  $\text{WS}_2$  sheets, a semiconductor-to-metal transition occurs. Comparing to the bulk compounds, these monolayer sheets have similar structural parameters and properties, but their vibrational and electronic properties are varied and have special characteristics. Our results suggest that the graphene-like  $\text{MX}_2$  sheets have potential applications in nano-electronics and nano-devices.

© 2011 Elsevier B.V. All rights reserved.

## 1. Introduction

Since the discovery of graphene [1,2], two-dimensional nanostructures have attracted lots of interests in nano-science and condensed matter physics [3–8]. Graphene is a monolayer carbon hexagonal sheet, which has a unique massless Dirac-like electronic excitation [3]. The two-dimensional graphene sheet is a semimetal, while for the graphene with finite width, it becomes a semiconductor or a half-metal depending on the edge shapes [4,5]. In the experiments, graphene sheets are initially obtained by micro-mechanical cleavage technique, using which the mono- and few-layer sheets are pulled from the layered graphite material [2]. Recently, several chemical methods, such as epitaxial growth on SiC surfaces, chemical vapor deposition on metal surfaces, reduction of graphite oxide, have been reported for the high-yield production of graphene [7–9]. Besides carbon-based nanostructures, other inorganic nanomaterials, especially whose structures are analogous to graphene, have also been synthesized and investigated [10]. For example, the two-dimensional BN sheet has been successfully

synthesized by the micro-mechanical cleavage technique and chemical-solution-derived method [11]. Through high-resolution transmission electron microscopy, it has been observed that B and N atoms occupy one sublattice of the hexagonal sheet, respectively [12]. Different from graphene, due to the inequivalence of the two sublattices, the two-dimensional BN sheet is a wide band-gap semiconductor [13].

Binary metal-dichalcogenides also have similar layered structures as graphite. By chemical bath deposition method and the mechanochemical route, the molybdenum disulfide ( $\text{MoS}_2$ ) films have been obtained in the experiments [14]. Besides, the two-dimensional  $\text{MoS}_2$  sheet has been reported by micro-mechanical cleavage as early as the time of graphene [2]. Recently, the monolayer  $\text{MoS}_2$  sheet has been successfully synthesized by chemical methods in the experiment [15]. Previous theoretical studies show that bulk  $\text{MoS}_2$  is an indirect-band-gap semiconductor [16,17], while the two-dimensional  $\text{MoS}_2$  sheet is a direct-band-gap semiconductor [18]. The  $\text{MoS}_2$  sheet could be rolled up into  $\text{MoS}_2$  nanotubes, which are all semiconductors regardless of the chirality [19]. While for the  $\text{MoS}_2$  sheets of finite width, the corresponding nanoribbons become ferromagnetic metals [20]. Similar to the  $\text{MoS}_2$  sheet, the graphene-like  $\text{WS}_2$  nanostructure has also been synthesized [15]. The corresponding  $\text{WS}_2$  nanotubes are also semiconductors [21]. From Landolt-Börnstein database [22], we find that the

\* Corresponding authors. Tel./fax: +86 057128865286.

E-mail addresses: dingyi2001@tsinghua.org.cn (Y. Ding), wangyanli-04@tsinghua.org.cn (Y. Wang).

MoSe<sub>2</sub>, MoTe<sub>2</sub>, NbS<sub>2</sub>, NbSe<sub>2</sub>, WS<sub>2</sub>, WSe<sub>2</sub>, TaS<sub>2</sub>, and TaSe<sub>2</sub> materials have the same layered structural type as that of MoS<sub>2</sub>. However, among those materials, previous studies have only been performed on the two-dimensional sheets of the MoS<sub>2</sub>, NbSe<sub>2</sub>, and WS<sub>2</sub> systems [15,18]. Thus, it is promising to perform a systemic study on those graphene-like sheets, which is helpful for the fabrications and applications of those nanomaterials.

In this paper, we investigate the structural, vibrational and electronic properties of the two-dimensional MX<sub>2</sub> (M=Mo, Nb, W, Ta; X=S, Se, Te) sheets by first principles calculations. The lattice parameters, charge transfers, cohesive energies, Raman active and infrared active vibrational modes, and the band gaps of the MX<sub>2</sub> sheets are obtained and compared to the bulk ones in detail. We also discuss the metal doping effects and predict a semiconductor-to-metal transition in the MoS<sub>2</sub> and WS<sub>2</sub> sheets.

## 2. Methods

The first principle calculations are performed by VASP with a plane-wave set and projector augmented wave pseudopotentials [23]. Two types of exchange and correlation (XC) functionals, the Ceperly–Alder functional form of the local density approximation (LDA) and the Perdew–Burke–Ernzerhof (PBE) functional form of the generalized gradient approximation (GGA) are adopted in the calculations. The plane-wave cutoff energy is set to be 400 eV. The supercells are used to simulate the isolated sheets and in order to avoid interlayer interactions, the distance between sheets is set to larger than 12 Å. The lattice constants and the atom coordinates are optimized until the convergence of the force on each atom is less than 0.01 eV/Å. The Monkhorst–Pack scheme is used to sample the Brillouin zone. The structures are fully relaxed with a mesh of 12 × 12 × 1, and the mesh of *k* space is increased to 15 × 15 × 1 and 24 × 24 × 1 in the static and density of state (DOS) calculations, respectively.

## 3. Results

### 3.1. Structural properties

The crystal structure of the monolayer MoS<sub>2</sub> sheet is shown in Fig. 1(a). Similar to BN, SiC, ZnO and other heterogeneous graphene-like sheets, Mo atoms occupy one sublattice of the hexagonal sheet and S atoms occupy the other. However, due to the chemical ratio of Mo:S=1:2, the Mo sublattice layer is sandwiched between two nearby S sublattice layers. We obtain the thickness of the MoS<sub>2</sub> sheet is 3.13 Å (3.12 Å) and the length of the Mo–S bond is 2.42 Å (2.39 Å) by the PBE (LDA) calculations. These calculated values agree well with the previous calculations by Li [20] and Ramakrishna Matte [15]. The optimized lattice constant of the MoS<sub>2</sub> sheet is 3.19 Å (3.13 Å) with PBE (LDA), which is almost the same as the bulk value of 3.15 Å [20].

All the lattice parameters of the MX<sub>2</sub> sheets are listed in Table 1. It can be seen that the MoX<sub>2</sub> and WX<sub>2</sub> sheets, the NbX<sub>2</sub> and TaX<sub>2</sub> sheets have quite similar lattice parameters. For the same chalcogen, the difference of metals affects the lattice parameters slightly. For example, the in-sheet lattice constants of NbS<sub>2</sub> and TaS<sub>2</sub> sheets are only 0.15 Å longer than those of the MoS<sub>2</sub> and WS<sub>2</sub> ones. Four disulfide sheet, MoS<sub>2</sub>, WS<sub>2</sub>, NbS<sub>2</sub>, and TaS<sub>2</sub> sheets, have a general thickness of 3.1 Å. However, different chalcogen atoms change the lattice parameters significantly. The diselenide and ditelluride sheets increase the thickness to 3.3 and 3.6 Å, respectively. Due to the increase of the chalcogen atomic radius, both the bond lengths *d*<sub>M–X</sub> and the in-sheet lattice constants also increase in the sequence of MS<sub>2</sub> < MSe<sub>2</sub> < MTel<sub>2</sub> for the same metal atoms.

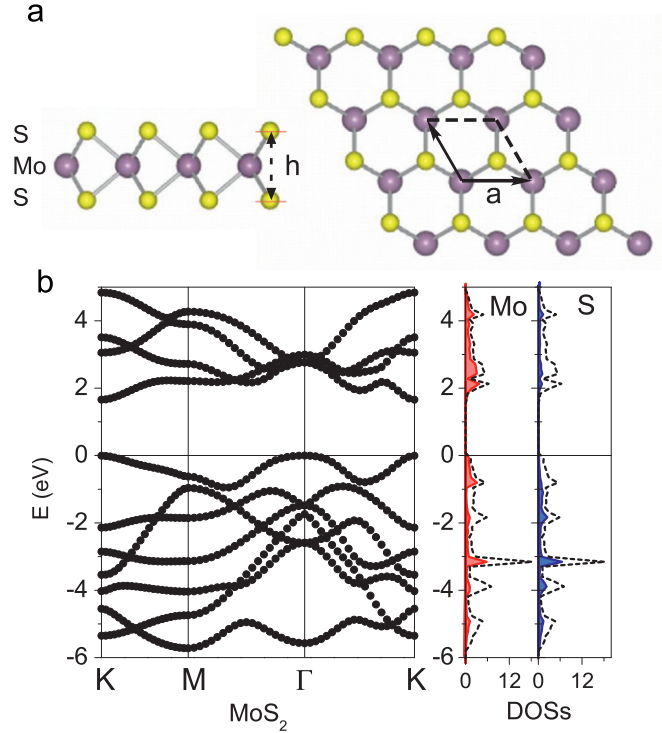


**Fig. 1.** (a) The side and top view of the graphene-like MoS<sub>2</sub> sheet. (b) The band structure, total and partial DOSs for the Mo d and S p orbitals. The dot lines represent the total DOSs of the MoS<sub>2</sub> sheet. The Fermi level is indicated as the line at *E* = 0.0 eV.

The difference of chalcogens affects not only the lattice parameters, but also the cohesive energies. In our calculations, the cohesive energies are defined as  $E_c(MX_2) = E_{MX_2} - E_{M\ atom} - 2 \times E_{X\ atom}$ . Here,  $E_{MX_2}$  is the total energy of the MX<sub>2</sub> sheet,  $E_{M\ atom}$  and  $E_{X\ atom}$  are the energies of the corresponding metal and chalcogen isolated atoms. When the cohesive energies are more negative, the MX<sub>2</sub> sheets are more favorable. For the MoS<sub>2</sub> sheet, our PBE calculations show the formation energy is −5.07 eV/atom, which is in accordance with the GGA result of −5.20 eV/atom and the pseudo-atomic numerical orbitals result of −5.00 eV/atom [20]. While the LDA calculations predict a larger value of −6.25 eV/atom. This phenomenon is common for the first principles calculations, since the LDA XC functional normally gets short lattices and high energies, while the GGA one has the contrary trends [24,25]. From Table 1, it can be seen that  $E_c(MS_2) < E_c(MSe_2) < E_c(MTe_2)$ . Using the Bader analysis [26], we obtain the charge transfers from the metal to the chalcogen atoms. As shown in Table 1, in the MoS<sub>2</sub> sheet, the Mo atom loses 0.90 e and each S atom gains 0.45 e. While in the MoSe<sub>2</sub> and MoTe<sub>2</sub> sheets, the charge transfers of Mo atoms decrease to 0.76 and 0.24 e, respectively. Due to the small charge transfers and elongated lattice constants, the cohesive energies of the MoSe<sub>2</sub> and MoTe<sub>2</sub> sheets decrease to −4.53 and −3.97 eV/atom, respectively. Since the W, Nb, and Ta atoms transfer more electrons to the chalcogen atoms than the Mo atoms, their corresponding sheets will have higher cohesive energies than the MoX<sub>2</sub> systems. We also calculate the formation energies of the MX<sub>2</sub> sheets as  $E_{form} = E_{MX_2} - E_{M\ bulk} - 2 \times E_{X\ dimer}$ . Here,  $E_{M\ bulk}$  and  $E_{X\ dimer}$  represent the atomic energies in their stable elemental structures. For the metals, the stable structure is a body-centered cubic (bcc) bulk with the Im-3m space group, while for the chalcogens, the stable structure is a molecular dimer. As shown in Table 1, all the MX<sub>2</sub> sheets have negative formation energies, which means the composing processes from the elemental forms are exothermic reactions and those MX<sub>2</sub> sheets are stable. The  $E_{form}$  of MoS<sub>2</sub> and

**Table 1**  
The lattice constants  $a$ , bond lengths  $d_{M-X}$ , sheet thicknesses  $h$ , cohesive energies  $E_c$ , formation energies  $E_{form}$ , charge transfers of metals  $\Delta Q$ , vibrational frequencies at the  $\Gamma$  point, and electronic properties of the  $MX_2$  ( $M=Mo, Nb, W, Ta$ ;  $X=S, Se, Te$ ) sheets. The PBE and LDA represent the XC functionals used in the calculations.

|                   |     | $a$ (Å) | $d_{M-X}$ (Å) | $h$ (Å) | $E_c$ (eV/atom) | $E_{form}$ (eV/atom) | $\Delta Q$ (e) | $E''$ (cm <sup>-1</sup> ) | $E'$ (cm <sup>-1</sup> ) | $A'_1$ (cm <sup>-1</sup> ) | $A'_2$ (cm <sup>-1</sup> ) |               |
|-------------------|-----|---------|---------------|---------|-----------------|----------------------|----------------|---------------------------|--------------------------|----------------------------|----------------------------|---------------|
| MoS <sub>2</sub>  | PBE | 3.19    | 2.42          | 3.13    | -5.07           | -1.42                | 0.90           | 276                       | 374                      | 396                        | 457                        | Semiconductor |
|                   | LDA | 3.13    | 2.39          | 3.12    | -6.25           | -1.71                | 0.86           | 290                       | 392                      | 411                        | 475                        | Semiconductor |
| MoSe <sub>2</sub> | PBE | 3.33    | 2.55          | 3.35    | -4.53           | -1.21                | 0.76           | 160                       | 277                      | 233                        | 343                        | Semiconductor |
|                   | LDA | 3.25    | 2.51          | 3.32    | -5.73           | -1.50                | 0.84           | 168                       | 291                      | 243                        | 359                        | Semiconductor |
| MoTe <sub>2</sub> | PBE | 3.56    | 2.74          | 3.62    | -3.97           | -0.86                | 0.24           | 114                       | 230                      | 167                        | 285                        | Semiconductor |
|                   | LDA | 3.47    | 2.69          | 3.60    | -5.13           | -1.14                | 0.24           | 120                       | 241                      | 174                        | 300                        | Semiconductor |
| WS <sub>2</sub>   | PBE | 3.19    | 2.42          | 3.14    | -5.71           | -1.37                | 1.00           | 287                       | 344                      | 409                        | 426                        | Semiconductor |
|                   | LDA | 3.13    | 2.39          | 3.13    | -6.90           | -1.65                | 0.98           | 300                       | 360                      | 423                        | 441                        | Semiconductor |
| WSe <sub>2</sub>  | PBE | 3.32    | 2.55          | 3.36    | -5.10           | -1.09                | 0.60           | 166                       | 238                      | 241                        | 298                        | Semiconductor |
|                   | LDA | 3.25    | 2.51          | 3.34    | -6.31           | -1.38                | 0.68           | 174                       | 249                      | 250                        | 311                        | Semiconductor |
| WTe <sub>2</sub>  | PBE | 3.56    | 2.74          | 3.63    | -4.46           | -0.66                | 0.19           | 118                       | 192                      | 172                        | 239                        | Semiconductor |
|                   | LDA | 3.47    | 2.70          | 3.61    | -5.63           | -0.95                | 0.24           | 124                       | 200                      | 180                        | 250                        | Semiconductor |
| NbS <sub>2</sub>  | PBE | 3.36    | 2.49          | 3.14    | -5.44           | -1.56                | 1.06           | 215                       | 295                      | 372                        | 373                        | Metal         |
|                   | LDA | 3.29    | 2.46          | 3.12    | -6.45           | -1.81                | 1.04           | 232                       | 315                      | 383                        | 389                        | Metal         |
| NbSe <sub>2</sub> | PBE | 3.48    | 2.62          | 3.37    | -4.92           | -1.37                | 0.90           | 123                       | 230                      | 221                        | 284                        | Metal         |
|                   | LDA | 3.41    | 2.58          | 3.34    | -5.96           | -1.63                | 0.92           | 131                       | 242                      | 228                        | 296                        | Metal         |
| NbTe <sub>2</sub> | PBE | 3.70    | 2.82          | 3.69    | -4.34           | -1.01                | 0.36           | 91                        | 199                      | 154                        | 241                        | Metal         |
|                   | LDA | 3.59    | 2.78          | 3.69    | -5.35           | -1.26                | 0.36           | 95                        | 199                      | 153                        | 260                        | Metal         |
| TaS <sub>2</sub>  | PBE | 3.34    | 2.48          | 3.13    | -5.92           | -1.60                | 1.12           | 230                       | 282                      | 355                        | 387                        | Metal         |
|                   | LDA | 3.28    | 2.47          | 3.10    | -6.87           | -1.85                | 1.10           | 242                       | 298                      | 368                        | 401                        | Metal         |
| TaSe <sub>2</sub> | PBE | 3.48    | 2.62          | 3.36    | -5.34           | -1.35                | 0.92           | 130                       | 198                      | 230                        | 251                        | Metal         |
|                   | LDA | 3.40    | 2.57          | 3.32    | -6.31           | -1.60                | 0.88           | 135                       | 209                      | 238                        | 261                        | Metal         |
| TaTe <sub>2</sub> | PBE | 3.71    | 2.82          | 3.66    | -4.67           | -0.91                | 0.34           | 94                        | 166                      | 164                        | 201                        | Metal         |
|                   | LDA | 3.61    | 2.77          | 3.64    | -5.62           | -1.15                | 0.34           | 97                        | 173                      | 169                        | 212                        | Metal         |

WS<sub>2</sub> sheets are -1.42 and -1.37 (-1.71 and -1.65) eV/atom by the PBE (LDA) calculations. Comparing the  $E_c$  and  $E_{form}$  of the  $MX_2$  sheets in Table 1, we find that the NbS<sub>2</sub> and TaS<sub>2</sub> sheets have higher cohesive and formation energies than the synthesized MoS<sub>2</sub> and WS<sub>2</sub> ones. It is possible to produce these sheets from their bulk structures by similar chemical methods for the MoS<sub>2</sub> and WS<sub>2</sub> materials [15].

### 3.2. Vibrational properties

For the low-dimensional nanostructures, Raman spectra is one important characterization tool in the experiments [27]. Recently, two groups have measured the Raman shift of the MoS<sub>2</sub> sheets [15,28]. Here, we use the finite displacements methods to investigate the zone-centered vibrational properties of the  $MX_2$  sheets. Since the  $MX_2$  monolayer has the symmetry of  $D_{3h}$  point group, besides three acoustic modes, the six optical modes at the  $\Gamma$  point can be classified as follows:  $\Gamma_{opt} = 2E''(R) + 2E'(I+R) + A'_1(R) + A'_2(I)$ . The  $R$  and  $I$  represent the vibrational modes having Raman and infrared activities, respectively. Fig. 2 shows the atomic displacements for each vibrational mode. The  $E''$  and  $E'$  modes represent the in-sheet movements of atoms, which are doubly degenerate due to the equivalence of  $x$  and  $y$ -axes. For the  $E''$  mode, only the chalcogen atoms move oppositely. The frequency of this mode is less than 300 cm<sup>-1</sup>, which is beyond the range of experimental measurements [15,28]. For the  $E'$  mode, two chalcogen atoms move in the same direction and the metal atom moves oppositely. The calculated frequency is 374 cm<sup>-1</sup> with PBE and 392 cm<sup>-1</sup> with LDA. Lee et al. measure the monolayer MoS<sub>2</sub> sample and obtain the  $E'$  mode is in the range of 381–385 cm<sup>-1</sup> [28]. Ramakrishna Matte et al. report a frequency of 379.7 cm<sup>-1</sup> for the MoS<sub>2</sub> film [15]. Comparing to these experimental values, the PBE calculation is underestimated, while the LDA one is overestimated. The  $A'_1$  and  $A'_2$  modes are non-degenerate. Both modes represent the out-sheet movements of

atoms as shown in Fig. 2(a). The  $A'_1$  mode is the Raman active vibration, whose frequency is 396 (411) cm<sup>-1</sup> for the PBE (LDA) calculations. In the experiments, Lee et al. obtain the  $A'_1$  mode is in the range of 401–407 cm<sup>-1</sup> [28], and Ramakrishna Matte et al. get a value of 404.7 cm<sup>-1</sup> [15]. Our calculated results agree well with these experimental values within 2% deviations. The  $A'_2$  mode is an infrared active frequency of about 460 cm<sup>-1</sup>, which needs further experimental verifications.

For other  $MX_2$  sheets, the corresponding vibrational frequencies are listed in Table 1. Since the  $E'$  and  $A'_1$  modes are usually measured in the experiments [15,28], we focus on these two modes for different  $MX_2$  sheets. The  $E'$  and  $A'_1$  modes of the WS<sub>2</sub> sheet are 344 (360) and 409 (423) cm<sup>-1</sup> by the PBE (LDA) calculations, which also agree well with the experimental results [15]. Since the movements of the chalcogen atoms contribute to the displacements mainly, the vibrational frequencies of the  $E'$  and  $A'_1$  modes are determined by the chalcogen atoms. Taking the MoX<sub>2</sub> sheets as an example, the  $E'$  mode of the MoSe<sub>2</sub> sheet decreases by about 100 cm<sup>-1</sup> compared to the MoS<sub>2</sub> sheet. The out-sheet vibrational frequency of the MoSe<sub>2</sub> sheet also decreases fast as shown in Fig. 2. The  $A'_1$  mode reduces to 233 cm<sup>-1</sup>, which becomes less than the  $E'$  mode. When the chalcogen atoms are the Te element, the MoTe<sub>2</sub> sheet has the  $E'$  and  $A'_1$  frequencies down to 230 and 167 cm<sup>-1</sup>, respectively. For other WX<sub>2</sub>, NbX<sub>2</sub>, TaX<sub>2</sub> systems, we also obtain that the frequencies of  $E'$  and  $A'_1$  modes follow the order of MS<sub>2</sub> > MSe<sub>2</sub> > MTe<sub>2</sub>.

### 3.3. Electronic properties

Although the difference of chalcogen atoms affects the structural and vibrational properties, it has little influence on the electronic properties. Figs. 1(c) and (d) show the electronic structure of the MoS<sub>2</sub> sheet. The MoS<sub>2</sub> sheet is a semiconductor with a direct-band gap at the  $K$  point. The PBE (LDA) gap value

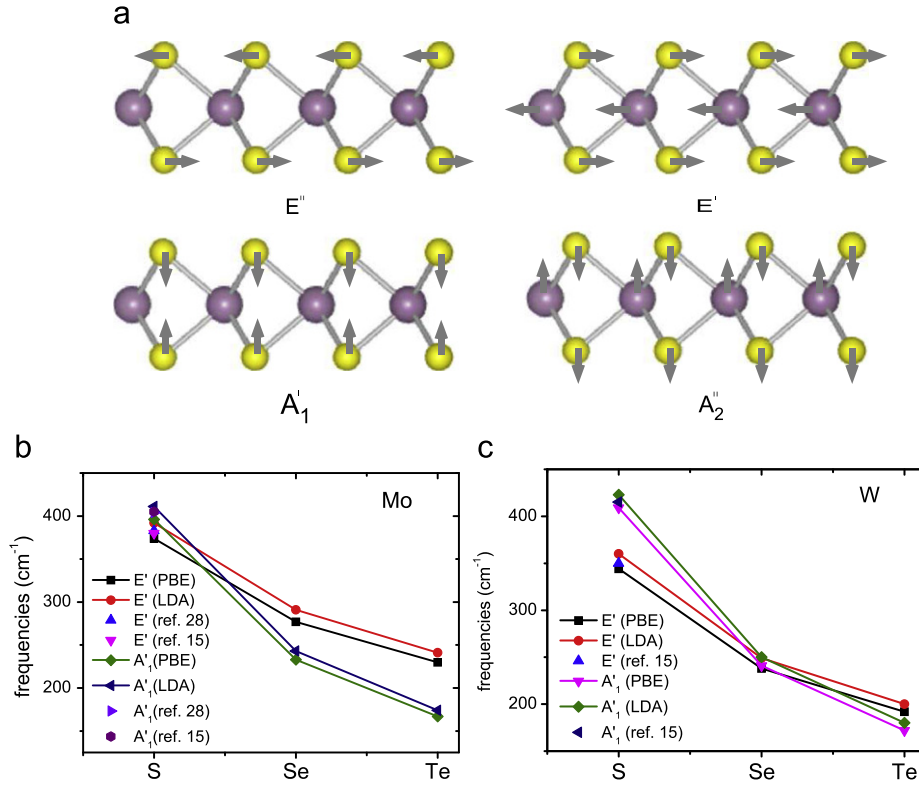


**Fig. 2.** (a) The vibrational modes of MX<sub>2</sub> sheets. Arrows in the figure represent directions of the atomic displacements for each mode. The vibrational frequencies of E' and A<sub>1</sub>' modes for (b) MoX<sub>2</sub> and (c) WX<sub>2</sub> sheets.

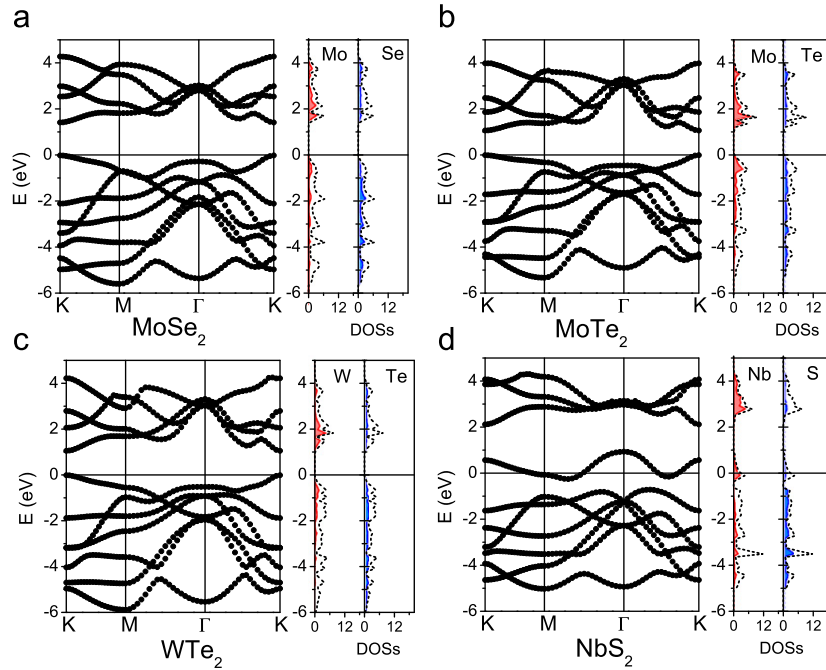


**Fig. 3.** The band structures, total and partial DOSs of the (a) MoSe<sub>2</sub>, (b) MoTe<sub>2</sub>, (c) WTe<sub>2</sub>, and (d) NbS<sub>2</sub> sheets.

is 1.67 (1.86) eV, which agrees well with the latest MoS<sub>2</sub> photoluminescence experiment [29] and previous theoretical studies [18,20]. Similar to the MoS<sub>2</sub> sheet, both the MoSe<sub>2</sub> and MoTe<sub>2</sub> ones are also direct-band-gap semiconductors as shown in Figs. 3(a) and (b). Fig. 3(c) displays the typical band structure of the WTe<sub>2</sub> sheet. For the three WX<sub>2</sub> sheets, we find they have analogous semiconducting properties. However, both the NbX<sub>2</sub>

and TaX<sub>2</sub> sheets become metals. As shown in Fig. 3(d), the NbS<sub>2</sub> sheet exhibits metallic behavior with one band crossing the Fermi level. The partial DOS analysis indicates this band is mainly attributed to the d orbitals of Nb atoms. Since the Nb (Ta) atom is one d electron less than the Mo (W) atom, the top d-character valence bands are not fully occupied and the metallicity appears in the NbX<sub>2</sub> (TaX<sub>2</sub>) sheets. This result is consistent with the



experimental observation that the TaS<sub>2</sub> films present robust metallic behaviors [30]. Thus, these metallic NbX<sub>2</sub> and TaX<sub>2</sub> sheets would be one type of conducting materials for nano-devices.

For the semiconducting MoX<sub>2</sub> and WX<sub>2</sub> sheets, the calculated PBE and LDA band gaps are listed in Table 2. It is well-known that the traditional DFT calculations perform well for the properties of the ground state, but generally underestimate the band gaps of materials [24]. In order to predict accurate band gaps, extra calculations are carried out by two ways. One way is utilizing the Heyd–Scuseria–Ernzerhof (HSE) hybrid XC functional. Comparing with the PBE results, the HSE calculations increase the band gaps by about 0.5 eV. The band gaps of the MoS<sub>2</sub> and WS<sub>2</sub> sheets are up

to 2.25 and 2.32 eV, respectively. The other way is doing the GW correction. The GW correction greatly increases the band gaps. As shown in Table 2, the MoX<sub>2</sub> and WX<sub>2</sub> sheets have the GW gaps ranging from 1.8 to 3 eV. However, no matter whether the traditional XC functional, hybrid XC functional, or GW correction is used, the band gaps of the MoX<sub>2</sub> and WX<sub>2</sub> sheets follow the same order of disulfide > diselenide > ditelluride. Considering that those direct-gaps are around 2–3 eV, the semiconducting MoX<sub>2</sub> and WX<sub>2</sub> sheets can be used as solar energy materials, luminescent materials, and so on.

Next, we consider the metal-doped effects on the MX<sub>2</sub> sheets. Since the MoS<sub>2</sub> and WS<sub>2</sub> sheets have been successfully fabricated [15] and the Nb atom can substitute Mo atom in the MoS<sub>2</sub> bulk material [31], we investigate four situations as the Nb-, W-doped MoS<sub>2</sub> sheet and the Ta-, Mo-doped WS<sub>2</sub> sheet. A 3 × 3 supercell is used, in which the distance between the doped atoms is larger than 9.5 Å. For the Nb-doped MoS<sub>2</sub> sheet, the formation energy is denoted as  $E_{\text{form}} = E_{\text{Nb-MoS}_2} - E_{\text{pure MoS}_2} - E_{\text{Nb atom}} + E_{\text{Mo atom}}$ . Here,  $E_{\text{Nb-MoS}_2}$  and  $E_{\text{pure MoS}_2}$  correspond to the total energies of Nb-doped and pure MoS<sub>2</sub> sheets, respectively. The  $E_{\text{form}}(\text{Nb-MoS}_2)$  is calculated to be −0.84 eV/unit. Similarly, we obtain  $E_{\text{form}}(\text{W-MoS}_2) = -1.93$  eV/unit,  $E_{\text{form}}(\text{Ta-WS}_2) = -0.38$  eV/unit, and  $E_{\text{form}}(\text{Mo-WS}_2) = 1.90$  eV/unit. The negative formation energies indicate the corresponding substitutional reactions could happen.

**Table 2**

The calculated band gaps at the *K*-point of the semiconducting MoX<sub>2</sub> and WX<sub>2</sub> sheets within different XC functionals of PBE, LDA, HSE, and GW correction.

|                   | PBE (eV) | LDA (eV) | HSE (eV) | GW (eV) |
|-------------------|----------|----------|----------|---------|
| MoS <sub>2</sub>  | 1.67     | 1.86     | 2.25     | 2.66    |
| MoSe <sub>2</sub> | 1.44     | 1.63     | 1.99     | 2.31    |
| MoTe <sub>2</sub> | 1.07     | 1.23     | 1.59     | 1.77    |
| WS <sub>2</sub>   | 1.81     | 1.94     | 2.32     | 2.91    |
| WSe <sub>2</sub>  | 1.55     | 1.74     | 2.10     | 2.51    |
| WTe <sub>2</sub>  | 1.06     | 1.14     | 1.55     | 1.79    |

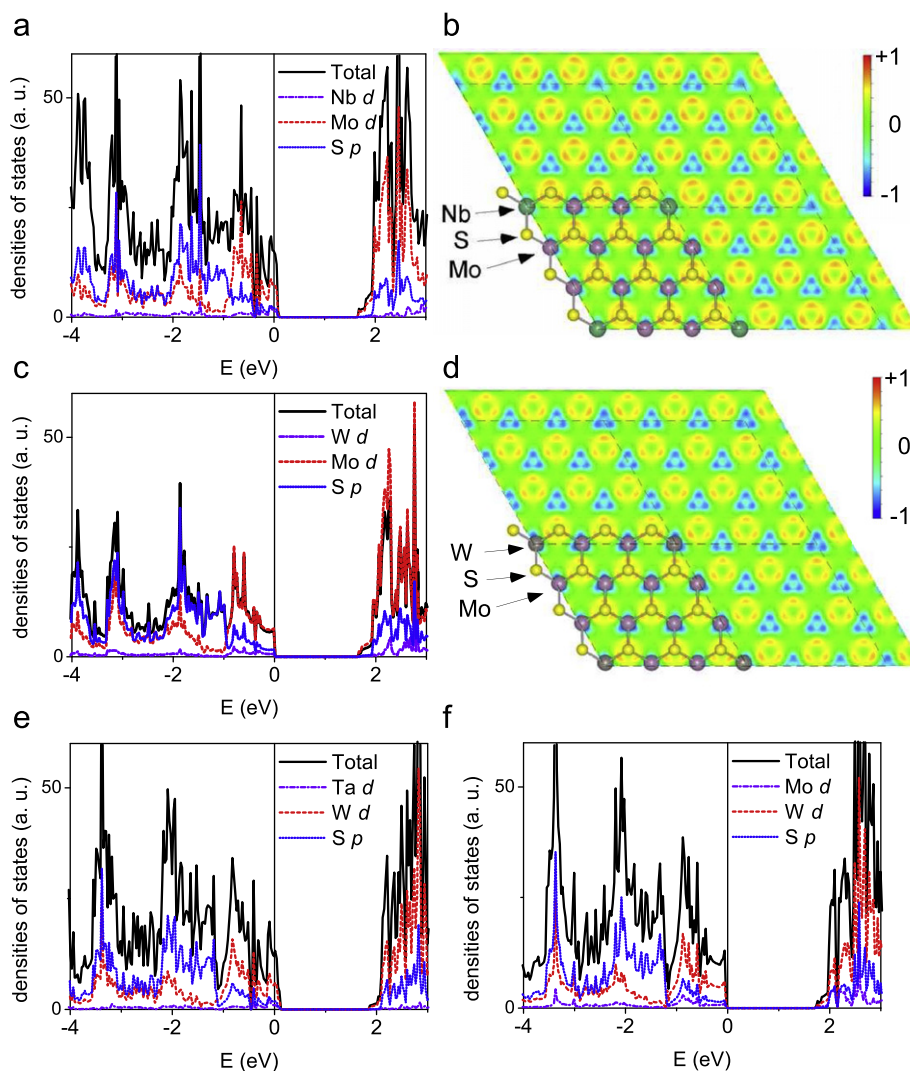


**Fig. 4.** (a and c) The total and partial DOSs of the Nb-doped and W-doped MoS<sub>2</sub> sheets. (b and d) The corresponding charge differences of the doping systems. (e and f) The total and partial DOSs of the Ta-doped and Mo-doped WS<sub>2</sub> sheets.

Thus, the Nb-doped MoS<sub>2</sub>, W-doped MoS<sub>2</sub> and Ta-doped WS<sub>2</sub> sheets are possible to be formed in the experiments. Fig. 4 shows the electronic properties of those doping systems. The Nb-doped MoS<sub>2</sub> sheet becomes a metal. From the charge difference in Fig. 4(b), we can see the Nb atoms lose more electrons than the Mo atoms. Considering the Nb atom is one d-electron less than the Mo atom, the Nb atoms act as holes doped in the MoS<sub>2</sub> sheet. It causes the downshift of the Fermi level and induces a semiconductor-to-metal transition in the MoS<sub>2</sub> sheet. While the W atoms behave quite similarly to the Mo atoms, little is changed after W doping in the MoS<sub>2</sub> sheet. The W-doped MoS<sub>2</sub> sheet is a semiconductor with a PBE band gap of 1.65 eV, which is almost identical to that of the pure MoS<sub>2</sub> sheet. In the WS<sub>2</sub> sheet, like the Nb-doped MoS<sub>2</sub> system, the Ta doping induces a semiconductor-to-metal transition shown in Fig. 4(e). While for the Mo doping, Fig. 4(f) displays the Mo-doped WS<sub>2</sub> sheet is still a semiconductor with a PBE band gap of 1.75 eV.

**Table 3**

The lattice constants  $a$  and  $c$  (Å), bond lengths  $d_{M-X}$  (Å), sheet thicknesses  $h$  (Å), cohesive energies  $E_c$  (eV/atom), formation energies  $E_{form}$  (eV/atom), charge transfers of metals  $\Delta Q$  (e), and vibrational frequencies at the  $\Gamma$  point (cm<sup>-1</sup>) of the bulk 2 H-like disulfide compounds. The PBE and LDA represent the XC functionals used in the calculations.

|                  |     | $a$  | $d_{M-X}$ | $h$  | $c$   | $E_c$ | $E_{form}$ | $\Delta Q$ | $E'$ | $A'_1$ |
|------------------|-----|------|-----------|------|-------|-------|------------|------------|------|--------|
| MoS <sub>2</sub> | PBE | 3.19 | 2.42      | 3.13 | 14.22 | -5.07 | -1.42      | 1.06       | 374  | 396    |
|                  | LDA | 3.13 | 2.39      | 3.12 | 12.09 | -6.29 | -1.75      | 1.03       | 389  | 411    |
| WS <sub>2</sub>  | PBE | 3.19 | 2.42      | 3.15 | 13.64 | -5.71 | -1.37      | 0.88       | 344  | 405    |
|                  | LDA | 3.13 | 2.39      | 3.13 | 12.13 | -6.93 | -1.69      | 1.00       | 357  | 423    |
| NbS <sub>2</sub> | PBE | 3.36 | 2.49      | 3.14 | 13.38 | -5.44 | -1.57      | 1.31       | 280  | 372    |
|                  | LDA | 3.29 | 2.46      | 3.12 | 11.88 | -6.50 | -1.86      | 1.20       | 307  | 388    |
| TaS <sub>2</sub> | PBE | 3.34 | 2.48      | 3.13 | 13.38 | -5.92 | -1.60      | 1.14       | 280  | 388    |
|                  | LDA | 3.27 | 2.45      | 3.11 | 11.98 | -6.92 | -1.89      | 1.13       | 293  | 400    |

#### 4. Discussions

Finally, we compare the structures and properties of the monolayer sheets to the bulk 2 H-like structures [16,20,31]. Table 3 shows the calculated results of bulk disulfide compounds. Since the PBE XC functional is hard to describe the van der Waals interactions between the layers, which give much longer lattice constants along the  $c$ -axis than the experimental values [22], we just compare the LDA results and find the similarities and differences of monolayer sheets to the bulks as following: (1) The sheets and bulks have similar structural properties. From Tables 1 and 3, it can be seen that the lattice parameters within the layered structure such as in-sheet constant  $a$ , bond length  $d_{M-X}$ , sheet thickness  $h$  are almost the same for the sheets and bulks. However, the metals transfer less charges to the S atoms in the sheets than in the bulks, which induces a little weaker cohesive energies for the monolayers. For the MoS<sub>2</sub> sheet, its  $E_c$  is 0.04 eV/atom lower than the bulk one. Similarly, the WS<sub>2</sub>, NbS<sub>2</sub>, and TaS<sub>2</sub> sheets also have a little smaller cohesive energies than the bulks. These energy differences between the bulks and monolayers are about 0.04–0.05 eV/atom. Comparing with the normal room temperature (0.025 eV), it indicates that producing the disulfide sheets from their bulk structures is energetically feasible. (2) The vibrational properties of sheets are different from the bulks. The  $E'$  frequencies of the bulks are all smaller than those in the sheets. While for the  $A'_1$  mode, the frequencies are nearly the same for the MoS<sub>2</sub> and WS<sub>2</sub> sheets and bulks, but for the NbS<sub>2</sub> and TaS<sub>2</sub> compounds, the frequencies of the monolayers are smaller than those of the bulks. In the experiments, those  $E'$  and  $A'_1$  modes have been used to distinguish the components and thickness of MoS<sub>2</sub> layers [28,32], and Lee et al. have reported that the  $E'$  mode softens, while the  $A'_1$  mode stiffens with the increase of the MoS<sub>2</sub> sample thickness [28]. Our calculated results are in accordance with this phenomenon, and predict the  $E'$  and  $A'_1$  modes for the NbS<sub>2</sub> and TaS<sub>2</sub> compounds will have stronger thickness dependence. (3) The electronic properties of sheets are also varied. Fig. 5 depicts the

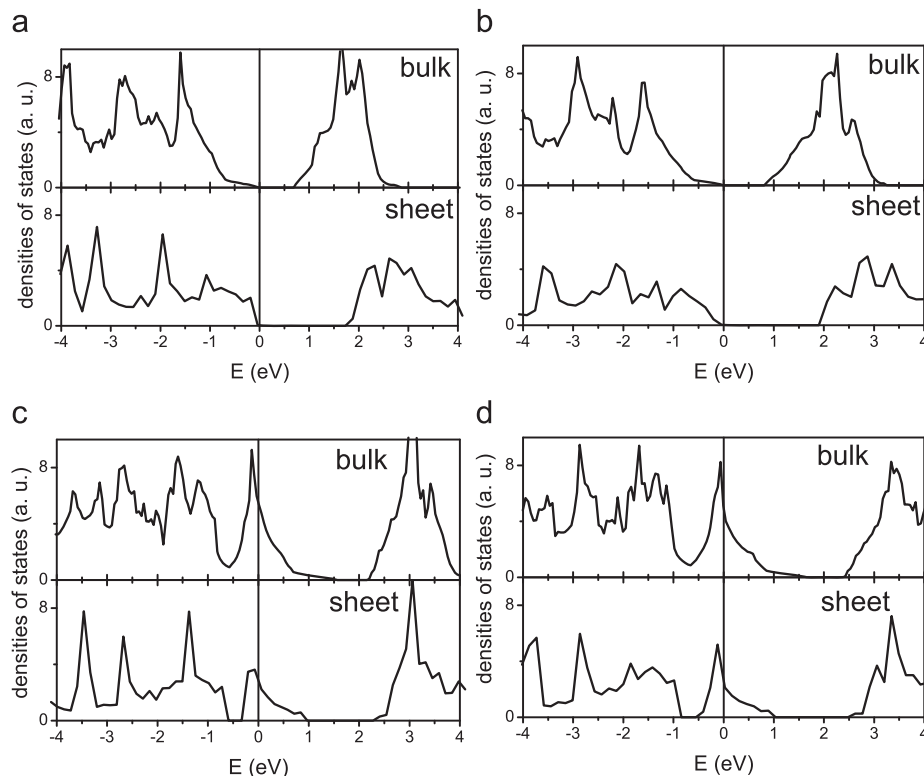


**Fig. 5.** The DOSs of bulk and monolayer MS<sub>2</sub> (M=Mo, W, Nb, Ta) compounds. (a) MoS<sub>2</sub>, (b) WS<sub>2</sub>, (c) NbS<sub>2</sub> and (d) TaS<sub>2</sub>.

electronic structures of bulk and monolayer disulfide compounds. The MoS<sub>2</sub> and WS<sub>2</sub> sheets have large direct-band gaps of 1.86 and 1.94 eV, respectively, while their corresponding bulks possess smaller indirect-band gaps of 0.74 and 0.86 eV. For the NbS<sub>2</sub> and TaS<sub>2</sub> compounds, although the sheets maintain the metallic behavior of the bulks, the DOSs of the sheets at the Fermi level are about half of those in the bulks as shown in Figs. 5(c) and (d).

## 5. Conclusions

In summary, we have investigated the structural, vibrational, and electronic properties of the graphene-like MX<sub>2</sub> monolayers by first principles calculations. We find that:

- (1) The NbS<sub>2</sub> and TaS<sub>2</sub> sheets are even more stable than the synthesized MoS<sub>2</sub> and WS<sub>2</sub> ones, which suggests it is possible to produce these sheets from their bulk structures by similar chemical methods for the MoS<sub>2</sub> and WS<sub>2</sub> materials.
- (2) The MoX<sub>2</sub> and WX<sub>2</sub> sheets have similar lattice parameters, vibrational modes, as well as electronic structures. Analogous relationships also exist between the NbX<sub>2</sub> and TaX<sub>2</sub> sheets. However, the MoX<sub>2</sub> and WX<sub>2</sub> sheets are semiconductors, while the NbX<sub>2</sub> and TaX<sub>2</sub> ones are metals.
- (3) The hybrid HSE functional and GW calculations show the semiconducting sheets have the band gaps of about 1.5–3 eV, which follow the order of MS<sub>2</sub> > MSe<sub>2</sub> > MTe<sub>2</sub>. When doping the Nb and Ta atoms into the sheets, a semiconductor-to-metal transition occurs in the MoS<sub>2</sub> and WS<sub>2</sub> systems.
- (4) Comparing to the bulk compounds, these monolayer sheets have similar structural parameters and properties, but their vibrational and electronic properties are varied. The semiconducting sheets have larger band gaps than the bulk compounds, and the metallic sheets have much smaller DOSs at the Fermi level than the bulk ones.

Our studies demonstrate that transition-metal dichalcogenide sheets, the inorganic analogs of graphene, have rich electronic structures for potential applications in nano-electronics, molecular sensing, and optical devices.

## Acknowledgments

Authors acknowledge the supports from HZNU (Grant No. 2011QDL016), ZSTU (Grant No. 0913847-Y), and NSFC (Grant No. 10974107). Y. Ding would like to thank Dr. Baoxing Li, Dr. Chao Cao, HZNU College of Science, and its HPC Center for helps.

## References

- [1] K.S. Novoselov, A.K. Geim, S.V. Morozov, D. Jiang, Y. Zhang, S.V. Dubonos, I.V. Grigorieva, A.A. Firsov, *Science* 306 (2004) 666.
- [2] K.S. Novoselov, D. Jiang, F. Schedin, T.J. Booth, V.V. Khotkevich, S.V. Morozov, A.K. Geim, *Proc. Natl. Acad. Sci. USA* 102 (2005) 10451.
- [3] A.H. Castro Neto, F. Guinea, N.M.R. Peres, K.S. Novoselov, A.K. Geim, *Rev. Mod. Phys.* 81 (2009) 109; A.K. Geim, *Science* 324 (2009) 1530.
- [4] Y.-W. Son, M.L. Cohen, S.G. Louie, *Nature (London)* (2006) 347.
- [5] M. Ezawa, *Eur. Phys. J. B* 66 (2008) 245; W.H. Liao, B.H. Zhou, H.Y. Wang, G.H. Zhou, *Eur. Phys. J. B* 76 (2010) 463.
- [6] L. Hu, X. Hu, X. Wu, C. Du, Y. Dai, J. Deng, *Physica B* 405 (2010) 3337; R. Thapa, D. Sen, M.K. Mitra, K.K. Chattopadhyay, *Physica B* 406 (2011) 368.
- [7] C.N.R. Rao, A.K. Sood, K.S. Subrahmanyam, A. Govindaraj, *Angew. Chem. Int. Ed.* 48 (2009) 7752.
- [8] S. Park, R.S. Ruoff, *Nat. Nanotechnol.* 4 (2009) 217.
- [9] M. Ye, Y.T. Cui, Y. Nishimura, Y. Yamada, S. Qiao, A. Kimura, M. Nakatake, H. Namatame, M. Taniguchi, *Eur. Phys. J. B* 75 (2010) 31.
- [10] R. Tenne, *Angew. Chem. Int. Ed.* 42 (2003) 5124; R. Tenne, *Nat. Nanotechnol.* 1 (2006) 103.
- [11] D. Pacilé, J.C. Meyer, C.Ö. Girit, A. Zettl, *Appl. Phys. Lett.* 92 (2008) 133107; W.-Q. Han, L. Wu, Y. Zhu, K. Watanabe, T. Taniguchi, *Appl. Phys. Lett.* 93 (2008) 223103.
- [12] C. Jin, F. Lin, K. Suenaga, S. Iijima, *Phys. Rev. Lett.* 102 (2009) 195505.
- [13] M. Topsakal, E. Aktürk, S. Ciraci, *Phys. Rev. B* 79 (2009) 115442; Y. Wang, *Phys. Status Solidi - Rapid Res. Lett.* 4 (2010) 34; S. Azevedo, J.R. Kaschny, C.M.C. de Castilho, F. de Brito Mota, *Eur. Phys. J. B* 67 (2009) 507.
- [14] K.M. Garadkar, A.A. Patil, P.P. Hankare, P.A. Chate, D.J. Sathe, S.D. Delekar, *J. Alloys Compd.* 487 (2009) 786; Z. Wu, D. Wang, A. Sun, *J. Alloys Compd.* 492 (2010) L5.
- [15] H.S.S. Ramakrishna Matte, A. Gomathi, A.K. Manna, D.J. Late, R. Datta, S.K. Pati, C.N.R. Rao, *Angew. Chem. Int. Ed.* 49 (2010) 4059.
- [16] R.A. Bromley, *Phys. Lett. A* 33 (1970) 242.
- [17] L. Wei, C. Jun-fang, H. Qinyu, W. Teng, *Physica B* 405 (2010) 2498.
- [18] S. Lebégue, O. Eriksson, *Phys. Rev. B* 79 (2009) 115409.
- [19] G. Seifert, H. Terrones, M. Terrones, G. Jungnickel, T. Frauenheim, *Phys. Rev. Lett.* 85 (2000) 146; I. Milosević, B. Nikolić, E. Dobardžić, M. Damnjanović, I. Popov, G. Seifert, *Phys. Rev. B* 76 (2007) 233414.
- [20] Y. Li, Z. Zhou, S. Zhang, Z. Chen, J. Am. Chem. Soc. 130 (2008) 16739; A.R. Botello-Méndez, F. López-Urías, M. Terrones, H. Terrones, *Nanotechnol. J.* 20 (2009) 325703.
- [21] G. Seifert, H. Terrones, M. Terrones, G. Jungnickel, T. Frauenheim, *Solid State Commun.* 114 (2000) 245; G. Seifert, H. Terrones, M. Terrones, T. Frauenheim, *Solid State Commun.* 115 (2000) 635.
- [22] Landolt-Börnstein database, Springer Publishing Company <<http://www.springermaterials.com>>, 2010.
- [23] G. Kresse, J. Furthmüller, *Comput. Mater. Sci.* 6 (1996) 15; G. Kresse, J. Furthmüller, *Phys. Rev. B* 54 (1996) 11169.
- [24] J. Hafner, *J. Comput. Chem.* 29 (2008) 2044.
- [25] P. Haas, F. Tran, P. Blaha, S. Pedrosa, J.R. da Silva, M. Odashima, K. Capelle, *Phys. Rev. B* 81 (2010) 125136.
- [26] W. Tang, E. Sanville, G. Henkelman, *J. Phys. Condens. Matter* 21 (2009) 084204.
- [27] M.S. Dresselhaus, G. Dresselhaus, R. Saito, A. Jorio, *Phys. Rep.* 409 (2005) 47.
- [28] C. Lee, H. Yan, L.E. Brus, T.F. Heinz, J. Hone, S. Ryu, *ACS Nano* 4 (2010) 2695.
- [29] A. Splendiani, L. Sun, Y. Zhang, T. Li, J. Kim, C.-Y. Chim, G. Galli, F. Wang, *Nano Lett.* 10 (2010) 1271.
- [30] A. Ayari, E. Cobas, O. Ogundadegbe, M.S. Fuhrer, *J. Appl. Phys.* 101 (2007) 014507.
- [31] V.V. Ivanovskaya, A. Zobelli, A. Gloter, N. Brun, V. Serin, C. Colliex, *Phys. Rev. B* 78 (2008) 134104.
- [32] D.O. Dumcenco, K.Y. Chen, Y.P. Wang, Y.S. Huang, K.K. Tiong, *J. Alloys Compd.* 506 (2010) 940.